Prussian Blue Analogues of Reduced Dimensionality

Gengler, Regis Y. N.; Toma, Luminita M.; Pardo, Emilio; Lloret, Francesc; Ke, Xiaoxing; Van Tendeloo, Gustaaf; Gournis, Dimitrios; Rudolf, Petra

Published in:
Small

DOI:
10.1002/smll.201200517

Publication date:
2012

Prussian Blue Analogues of Reduced Dimensionality

Régis Y. N. Gengler, Luminita M. Toma, Emilio Pardo, Francesc Lloret, Xiaoxing Ke, Gustaaf Van Tendeloo, Dimitrios Gournis,* and Petra Rudolf**

***M**ixed-valence polycyanides (Prussian Blue analogues) possess a rich palette of properties spanning from room-temperature ferromagnetism to zero thermal expansion, which can be tuned by chemical modifications or the application of external stimuli (temperature, pressure, light irradiation). While molecule-based materials can combine physical and chemical properties associated with molecular-scale building blocks, their successful integration into real devices depends primarily on higher-order properties such as crystal size, shape, morphology, and organization. Herein a study of a new reduced-dimensionality system based on Prussian Blue analogues (PBAs) is presented. The system is built up by means of a modified Langmuir–Blodgett technique, where the PBA is synthesized from precursors in a self-limited reaction on a clay mineral surface. The focus of this work is understanding the magnetic properties of the PBAs in different periodic, low-dimensional arrangements, and the influence of the "on surface" synthesis on the final properties and dimensionality of the system.*

1. Introduction

Mixed-valence polycyanides (Prussian Blue analogues, PBAs) possess a rich palette of properties spanning from room-temperature ferromagnetism[1–4] to zero thermal expansion,[5] which can be tuned by chemical modifications or the application of external stimuli (temperature,[6,7] pressure,[8] light irradiation[9,10]). In recent years, low-dimensional assemblies have assumed remarkable importance due to their outstanding physical, chemical, and biological properties which make them attractive for photophysical and electrical applications as well as for catalysis, molecular separation, drug delivery, and biosensing.[11] The control of both the organization of the assemblies and their properties through simple external parameters, has led to the creation of new tailored functional materials.[12] Using a bottom-up approach and exploiting a fundamental interaction to trigger self-assembly, one can create entirely novel molecular building blocks and form supramolecular architectures, whose final structure is encoded in the shape and properties of the clusters or molecules used. The family of molecule-based magnetic materials comprising single-molecule magnets such as Mn_{12} (0D),[13,14] 1D single-chain magnets,[15,16] 2D frameworks, and the broad range of 3D PBAs,[17] are of interest in this context. All these systems are built in a bottom-up approach, where the final properties of the materials are fine-tuned through a carefully considered choice of elementary building blocks (morphochemistry). Herein we use a method based on one of the most common—though not widely used—materials, namely layered smectite clay. Single clay platelets serve as templates for creating highly ordered low-dimensional assemblies of

Dr. R. Y. N. Gengler, Dr. L. M. Toma, Prof. P. Rudolf
Zernike Institute for Advanced Materials
University of Groningen
Nijenborgh 4, NL-9747AG Groningen, The Netherlands
E-mail: p.rudolf@rug.nl
Dr. E. Pardo, Prof. F. Lloret
Instituto de Ciencia Molecular (ICMol)/Departament de Química Inorgànica, Universitat de València
Edificios Institutos de Paterna
Catedrático José Beltrán Martínez n 2, 46980 Paterna, Spain
E-mail: francisco.lloret@uv.es
Dr. X. Ke, Prof. G. Van Tendeloo
EMAT research group
University of Antwerp
Groenenborgerlaan 171, B-2020 Antwerpen, Belgium
Prof. D. Gournis
Department of Materials Science and Engineering
University of Ioannina
GR-45110 Ioannina, Greece
E-mail: dgourni@uoi.gr

DOI: 10.1002/smll.201200517

NANO MICRO small

nanostructured systems in thin-film form. One of the key properties of smectite clays, essential to our study, is the ion-exchange capacity which relates to the number of cations (present at the clay surface for charge neutrality reasons) exchangeable with other positively charged species. As suggested by Umemura,[18] the aluminosilicate surface regulates the topology of the interacting molecules and affects possible supramolecular rearrangements or reactions, such as self-assembly processes, that are not easily controlled in solution. Recently a new method[18] combining self-assembly and Langmuir–Schaefer deposition has enabled the creation of a new type of clay hybrid grown layer-by-layer. The spatial arrangement of the clay platelets affords a higher control at the nanoscale level and an enhanced order at the macroscale level. Although this emerging field of clay nanoscience is still mostly unexplored, several studies have demonstrated the successful integration of a variety of guest species within the clay thin-film structure either synthesized in-situ on the clay surfaces (through cation-exchange and self-assembly processes) or via the integration of as-made functional molecules.[19–25]

In this work, we report on an innovation in the field of coordination chemistry. Applying our approach of in-situ "on surface" synthesis of PBAs (which, when synthesized in solution, form 3D magnetically ordered networks), a nanostructured thin-film, where PBA is sandwiched between clay platelets, is obtained. This arrangement reduces the PBA dimensionality from 3D to 2D and affords new spin-glass properties at ~65 K.

1.1. Materials

Similarly to the films prepared by modified Langmuir–Schaefer deposition described in the literature,[26] the hybrid films contain dimethyldioctadecylammonium (DODA) bromide as amphiphilic cation and montmorillonite (Kunipia F) as clay mineral. The air stable PBAs $Cs^{I}[Ni^{II}Cr^{III}(CN)_6]$ and $Cs^{I}[Mn^{II}Cr^{III}(CN)_6]$,[2–5] which show a high Curie temperature (T_C) of 90 K when synthesized in solution, were chosen as magnetic materials. DODA (Sigma Aldrich) was used as received and dissolved in a mixed solvent of HPLC-grade chloroform and methanol (9:1 in volume) to prepare a spreading solution of 0.1 mg mL^{-1}.

The smectite clay mineral was a sodium-saturated montmorillonite Kunipia F acquired from Kunimine Industries Co. (Japan) with the mineralogical formula $Ca_{0.11}Na_{0.891}(Si_{7.63}Al_{0.37})(Al_{3.053}Mg_{0.65}Fe_{0.245}Ti_{0.015})O_{20}(OH)_4$ calculated from the chemical analysis. The cation-exchange capacity (CEC) of the clay was 1.15 mequiv g^{-1}. The thickness of the single clay platelet, estimated from the crystal structure, is 9.6 Å. A stock suspension of the clay was prepared by stirring for 12 hours 1 g of clay in 1 L of Millipore ultrapure water (18.2 MΩ) and diluted to a given concentration just before used as a subphase in the Langmuir Blodgett trough.

For the "on surface" synthesis of PBA we employed as precursors (a) $NiCl_2 \bullet 6H_2O$, (b) $MnCl_2 \bullet 4H_2O$, (c) CsCl, and (d) $K_3[Cr(CN)_6]$. All those compounds were of the highest purity commercially available (Sigma Aldrich) and used as received. Together (a), (c),and (d) were used to prepare $Cs^{I}Ni^{II}[Cr^{III}(CN)_6]$ (shortly written as CsNiCr), (b), (c), and (d) to synthesize $Cs^{I}Mn^{II}[Cr^{III}(CN)_6]$ (shortly written as CsMnCr), and (a), (b), (c), and (d) for the fabrication of $Cs^{I}Ni^{II}[Cr^{III}(CN)_6]$-$Cs^{I}Mn^{II}[Cr^{III}(CN)_6$ (shortly written as CsNiMnCr).

Diamagnetic Mylar substrates of 0.125 mm thickness (from GE Polymershapes HiFi Snij-Unie) were used for X-ray diffraction, X-ray photoelectron spectroscopy, atomic force microscopy, high-resolution transmission electron microscopy, high-angle annular dark field scanning electron transmission microscopy, energy dispersive X-ray spectroscopy and magnetic measurements, while Calcium Fluoride (CaF_2) plates (15 mm × 10 mm × 1 mm), rendered hydrophobic by rubbing with molten ferric stearate (purchased from Sorem, France), were used as substrate for the FT-IR measurements.

1.2. Film Preparation

Films were prepared following the deposition cycle as depicted in the **Scheme 1** with the help of a thermostated Nima Technology 612D Langmuir–Blodgett (LB) trough at a temperature of 21 ± 0.5 °C. The surface tension in the trough was monitored with a Wilhelmy plate. Clay suspensions in 18.2 MΩ Millipore ultrapure water were used as subphase (as described above). A clay concentration in the suspension of 10 ppm was chosen as the optimal value.[26] To achieve the hybridization of the clay platelets, 200–300 μL of DODA - solvent mixture (0.1 mg mL^{-1}) were spread onto the water surface. After a waiting time of 15 min to allow for the solvent evaporation and the clay-surfactant functionalization to occur,[26–28] the hybrid DODA-clay layer was compressed at a rate of 30 cm min^{-1} until the chosen stabilization pressure of 14 mN m^{-1} was reached. This pressure was maintained throughout the deposition process. Films were transferred onto the hydrophobic substrate by horizontal dipping, with downward and lifting speeds of 10 mm min^{-1} and 2, respectively. Each time the substrate was lowered into the LB trough, it was allowed to touch the air-water interface in a very gentle dip of max 0.5 mm below the water level and then rinsed several times by dipping into ultrapure water. The exchangeable cations (i.e., Na^+) present on the outer surface of the transferred hybrid DODA-clay film were then ion-exchanged by dipping the film into an aqueous solution (50 mM) of another cationic compound, in our case Ni^{2+} for the synthesis of CsNiCr or Mn^{2+} for that of CsMnCr. The sample was rinsed copiously with pure water and subsequently immersed for 1 min in an aqueous solution containing $K_3[Cr(CN)_6]$ (50 mM) and an excess of CsCl (0.5 M) to induce the in-situ formation of a low-dimensional structure of CsNiCr or CsMnCr. The final surface was rinsed again copiously with pure water and dried by blowing with N_2. CsNiMnCr samples were prepared by following initially the procedure as described for CsNiCr, but after the formation of the CsNiCr layer, the film was dipped in the aqueous solution of Mn^{2+}, rinsed with pure water and dipped for 1 min in the aqueous solution of $K_3[Cr(CN)_6]$ and CsCl and rinsed again with pure water. To deposit multilayer films, one simply repeats the whole cycle as many times as needed (see Scheme 1).

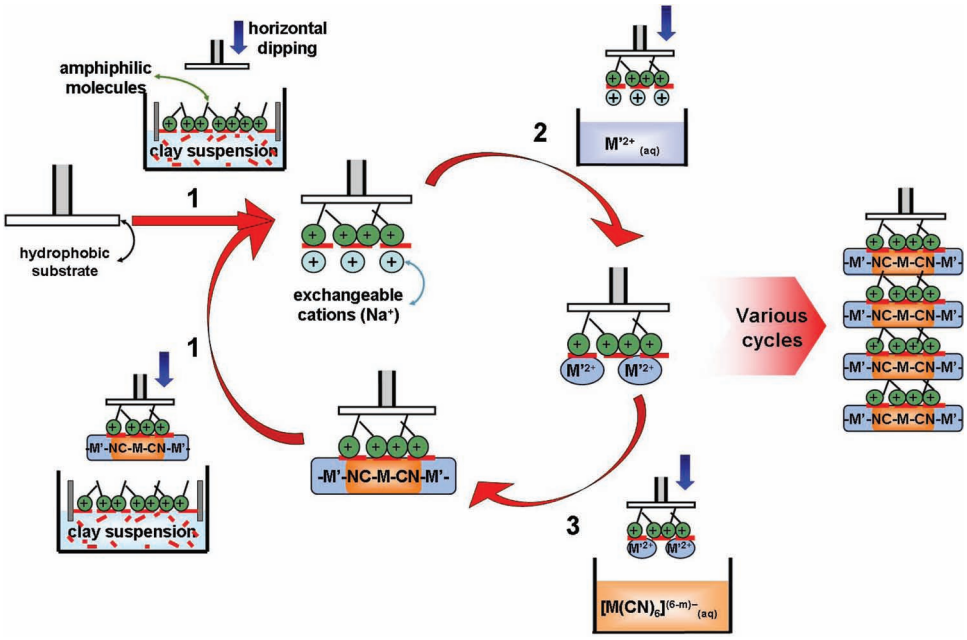

Scheme 1. Deposition procedure.

2. Characterization Tools

X-Ray diffraction (XRD) patterns were collected using a Philips PANanlytical X'Pert MRD diffractometer with a Cu Kα (λ = 1.5418 Å) radiation source (40 kV, 40 mA), a 0.25° divergent slit and a 0.125° antiscatter slit. The reflectivity patterns were recorded in the 2-theta (2θ) range from 0.5 to 10° with a 0.01° step and a counting time of 10 s per step.

X-ray photoelectron spectroscopy (XPS) data were collected with a SSX-100 (Surface Science Instruments) spectrometer equipped with a monochromatic Al Kα X-ray source ($h\nu$ = 1486.6 eV) and operating at a base pressure of 3×10^{-10} mbar. The energy resolution was set to 1.3 eV and the photoelectron take-off angle was 37°. A flood gun providing 0.1 eV kinetic energy electrons in combination with a Mo grid placed above the sample was used to compensate for sample charging. Binding energies are reported ±0.1 eV and referred to the Si 2p peak of clay at 102.9 eV.[29]

High-resolution transmission electron microscopy (HRTEM), high angle annular dark field scanning electron transmission microscopy (HAADF-STEM) and energy dispersive X-ray spectroscopy (EDX) data were collected using a FEI Tecnai G^2 microscope operated at 200 keV.

The infrared (IR) spectra were recorded in transmission mode with a Bruker IFS 66 v/S vacuum FTIR spectrometer operating at 10^{-2} mbar. The FTIR spectrometer was equipped with a liquid nitrogen cooled MCT detector and a KBr beam splitter. Each spectrum was the average of 150 scans collected with 2 cm^{-1} resolution.

Magnetic properties of DODA–clay–PBA hybrid films were investigated by carrying out variable temperature (2–300 K) DC magnetic measurements with a Quantum Design SQUID magnetometer. Variable-temperature (20–90 K) AC magnetic measurements were performed under zero applied static field and at 1 G oscillating field in the frequency range 1–1000 Hz.

3. Results and Discussion

X-ray diffraction patterns of hybrid multilayers were recorded in order to determine the d(00l) basal spacing of the hybrid DODA–clay–PBA structure. **Figure 1** (left) displays the XRD patterns of a 120-layer thick film of DODA–clay–PBA deposited on Mylar, where PBA stands for CsNiCr; CsMnCr and CsNiMnCr. For all three samples one observes multiple peaks, which clearly reveal an out-of-plane order in the film. Assuming that the first peak on each diffractogram represents the (001) Bragg peak, we can deduce from its position the dimensions of the repeating unit along the direction normal to the film plane. While for a structure without PBA consisting of DODA–Clay–DODA, d(001) = 35–36 Å,[26] a somewhat increased d spacing is observed for the three PBA containing samples, namely for CsNiCr 36.4 ± 0.5 Å, for CsMnCr 36.4 ± 0.5 Å, and for CsNiMnCr 37.6 ± 0.5 Å. The DODA–clay–PBA structure thus displays this slightly larger spacing notwithstanding the fact that the repeating unit contains just one layer of DODA per clay layer, contrary to the organoclay film without the PBA, where DODA is grafted on both sides of each clay platelet.[26] We can therefore reasonably assume that the repeating structure corresponds to the one displayed in Figure 1 (right panel): a single clay platelet of 9.6 Å thickness, a DODA layer of 15–20 Å thickness,[26] and a PBA layer of 7–12 Å thickness.

From this result one has to conclude that the PBA synthesized on the surface of the clay has a low dimensional structure (further evidence comes from HRTEM as discussed below). Yamamoto et al.[30–32] proposed that the structure of such a material deposited in-situ on the clay surface through cation-exchange was purely one-dimensional. According to these authors, PBA does not form a "perfect" 2D grid network, as the one shown in **Figure 2**A (note that the Cs ions are not shown for clarity) but rather isolated wire- or rod-like

NANO MICRO small

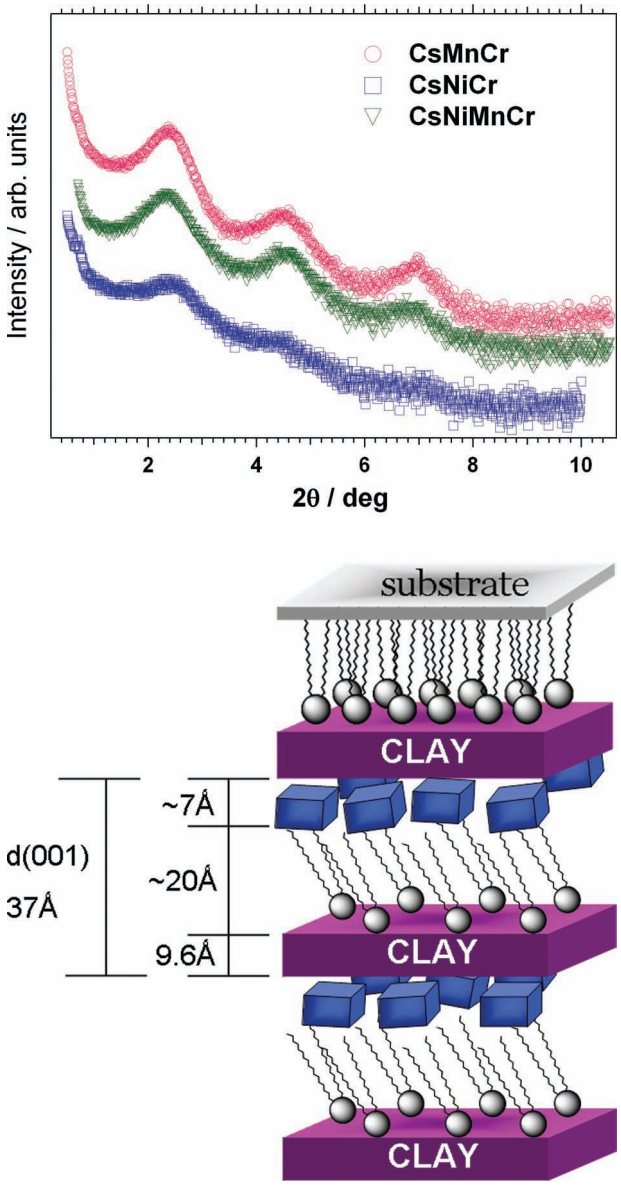

Figure 1. Top panel: X-ray diffraction patterns for 120-layer thick hybrid DODA–clay–PBA films where the PBA is (■) CsNiCr (1), (●) CsMnCr (2) and (▼) CsNiMnCr (3). Bottom panel: Model for the structure of a DODA–clay–PBA film where the Prussian blue units are represented by cubes between the clay–surfactant layers.

structures of alternating metal ions linked through cyano ligands (omitted for clarity in Figure 2). We can also exclude the possibility of a 3D-like network, as sketched in Figure 2C, since such a structure would imply a larger repeating unit as well as PBA-derived peaks in the diffractogram (not observed in our samples, see Figure S3 of the Supporting Information (SI)).

Moreover, since the material was assembled, as depicted in Scheme 1, in a sequence alternating two dips to synthesize the PBA with the DODA-clay dip (in the LB trough), it is unlikely that a 3D cubic structure forms under such circumstances. A structure like the one sketched in Figure 2D is equally unlikely for the same reasons, except if the primary M^{II} cations were mobile on the clay surface during the deposition. We therefore suggest that the PBA layer is either 1D- or 2D-like, as suggested by Yamamoto et al.[30–32] or, and equally likely, 2D- or 3D-like as displayed in Figure 2E. As already pointed out in previous studies of similar materials, gaining insight in the in-plane structure of the material deposited in the clay stack is a delicate task. Due to its low dimensionality and short range order along the X and Y axis, getting in plane crystallographic data is extremely difficult. Cs^+ cations, present in excess in the solution of $[Cr(CN)_6]^{3-}$, will be incorporated in the structure when the neutrality reasons require it.

X-ray photoelectron spectroscopy was applied to confirm the successful insertion of PBA between the clay platelets. As displayed in Scheme 1, the synthetic procedure involves successive dipping in aqueous solutions of $M^{II}Cl_2 \bullet nH_2O$ [where M^{II} = Ni and Mn, respectively, n = 6 (Ni^{II}) and 4 (Mn^{II})] and a mixed solution of $K_3[Cr(CN)_6]$ and CsCl in excess. It is expected that the M(II) cations will ion-exchange the Na^+ cations naturally present on the clay surface. Cl^- and Na^+, the side products of this reaction, should be eliminated in the rinsing step and not present in the film. Similarly $K_3Cr(CN)_6$ will react with the cation and release K^+ as side product, which in large measure are eliminated by rinsing. The successful integration of all the desired components in the hybrid films (DODA, clay and PBA) is confirmed by the elemental composition deduced from XPS. The overview spectrum shown in **Figure 3** for the case of CsNiCr features the fingerprint of all the expected constituents of the films: Al, Si, O (from the clay mineral) C, N (from the surfactant and the cyano ligands), Cr, Cs, Ni (from the PBA units). In addition to the elements mentioned, some K^+ ions from $K_3Cr(CN)_6$ are present in the film; presumably this residual potassium is due to limited amount of reactant [M(II)] cations on the clay surface given by the CEC as discussed above. Detailed scans of the metal core level regions are displayed at the bottom of Figure 3 and confirm the expected valency of the transition metal ions. This analysis is confirmed by STEM-EDX (see SI Figure S2) where all the elements specified above were detected.

HRTEM and high-angle annular dark-field scanning electron transmission microscopy (HAADF-STEM) analysis performed on the 120-layer hybrid films of DODA-clay-CsNiMnCr confirm the proposed model of bidimensional PBA growth through the "on surface" synthesis. The films were deposited on mylar and a ultra-thin cross-sectional lamella was prepared by a focused ion beam (FIB) to allow for TEM analysis. The HRTEM image (**Figure 4**a) clearly testifies a layered structure. The periodicity of the structure is in agreement with the crystallographic data provided by XRD and our proposed structure (Figures 1 and 2). Figure 4b shows a HAADF-STEM image of the same lamella where the layered structure is confirmed by a clear contrast between dark and brighter regions. Since HAADF-STEM is sensitive to the Z number of contributing elements, the brighter contrast in Figure 4b is due to the atoms with higher atomic number Z (Cs,Mn,Ni,Cr) present in PBA. The HAADF-STEM image therefore confirms that the PBA (higher Z) sandwiched between clay layers (low Z) is present as a 2D layer. In addition, an attempt of (in plane) diffraction using selected-area electron diffraction (SAED) did not yield evidence for

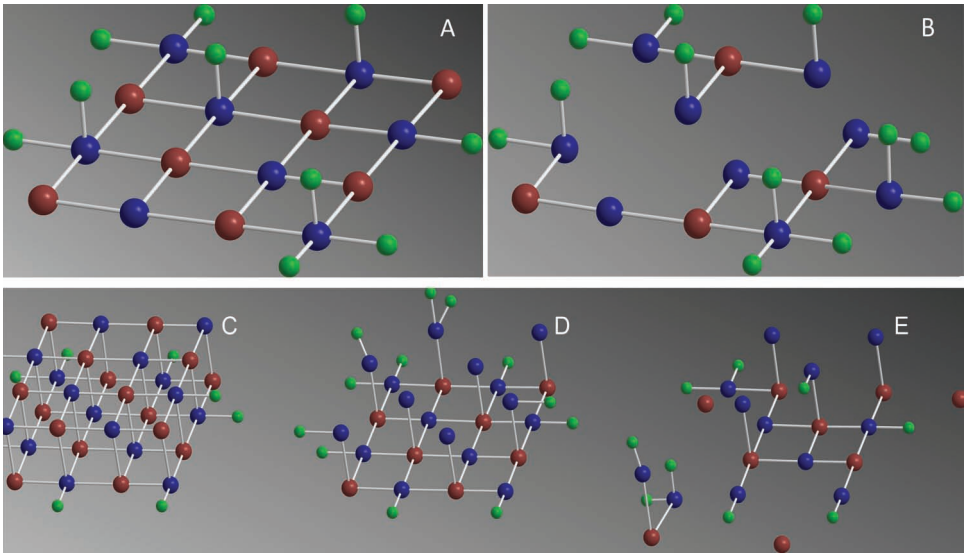

Figure 2. Proposed structural models for the low dimensional PBA compounds: blue balls = Cr^{III} ions, red balls = M^{II} ions (M = Ni, Mn), green balls = unreacted K ions (see discussion XPS results in main text).

PBA crystallites, once more rejecting the hypothesis that 3D PBA nano- or micro-crystallites are present in the films.

The infrared (IR) spectra of the 40-layer thick DODA–clay–PBA hybrid films deposited at 10 mN m^{-1} on CaF_2 substrate are shown in **Figure 5**. The FT-IR absorption spectra give some characteristic stretching vibration bands: the peaks at 2915 cm^{-1}, 2848 cm^{-1}, and 1466 cm^{-1} correspond to the symmetric and asymmetric stretching or scissoring vibrations of the methylene groups of dimethyldioctadecylammonium, the bands at 1116 cm^{-1} and 1035 cm^{-1} are assigned to the in-plane and out-of-plane ν(Si–O) vibrations of the montmorillonite clay, while the CN-bridged stretching bands appear at 2172.5 cm^{-1} (CsNiCr), 2162.0 cm^{-1} (CsMnCr), and 2166.5 cm^{-1} (CsNiMnCr). This once more indicates that all the components (clay platelets, amphiphilic surfactant, and PBAs) are present in the film. Moreover, as the number of hybrid layers increases, the intensity of the ν(CN) peaks of the DODA–clay–CsNiCr sample becomes more intense, as illustrated in Figure 5b, and their amplitudes grow linearly with the number of layers (inset Figure 5b); this confirms that the multilayer film of DODA, clay, and PBA is built up in a layer-by-layer fashion.

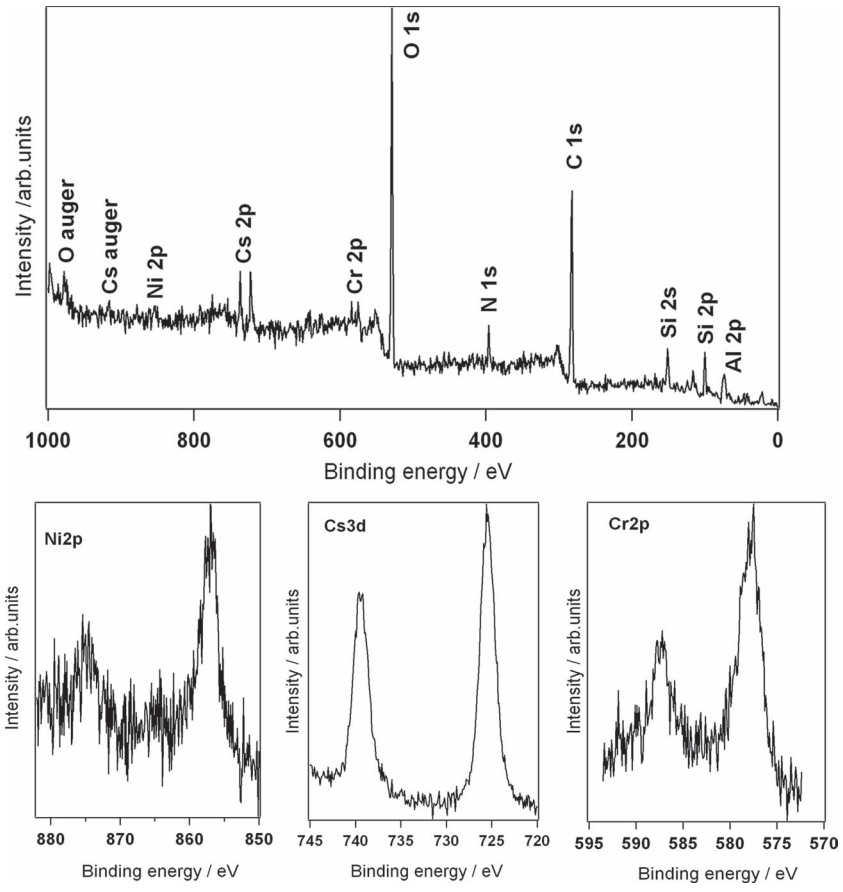

Figure 3. X-ray photoelectron spectra of a 40 layer thick hybrid DODA–clay–CsNiCr film, wide scan (top) and detailed scans of the Ni 2p, Cr 2p, and Cs 3d regions (bottom).

Normally the magnetic properties of a material are discussed based on the determination of the absolute intensity of magnetization. In the case of our films, the magnetically active material that is synthesized depends on the interaction with the clay and the ion-exchange; hence an absolute measurement of the total amount of PBA formed within the film structure could not be determined. Moreover, the nature of the film samples results in a significant diamagnetic background arising from the DODA-clay layers, substrate

small NANO MICRO

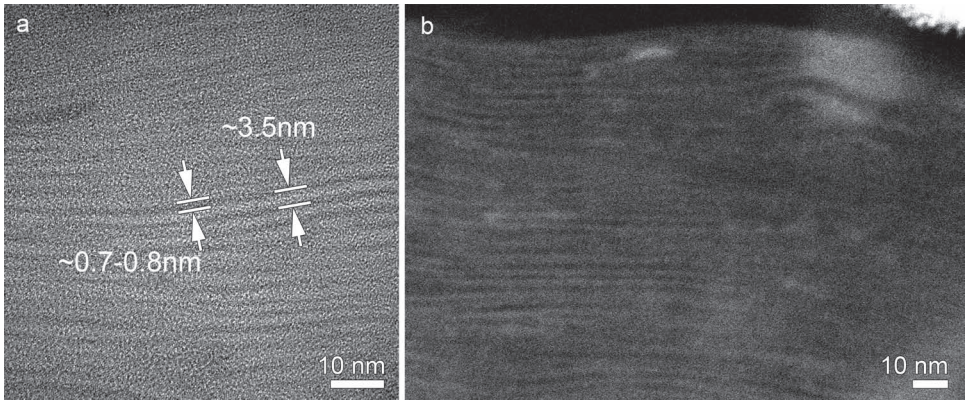

Figure 4. HRTEM (a) and HAADF-STEM image (b) of a cross-sectional thin lamella prepared from a 120-layer thick hybrid DODA–clay–CsNiMnCr film by a focussed ion beam.

and sample container, making it difficult to quantify the film response under external magnetic fields. Therefore, the magnitude of the magnetization will be given in arbitrary units.

The temperature dependence of the magnetization was recorded in field cooled (FC) and zero field cooled (ZFC) configuration in order to determine the Curie temperature, T_C, defined by the onset of the magnetization. The measurements of the magnetization versus temperature were performed with the external field both parallel and perpendicular to the film plane. The field-cooled magnetic response of the films is clearly anisotropic, being the parallel magnetization more intense than the perpendicular one. This magnetic anisotropy of the thin-film samples containing the Cr-CN-Ni and Cr-CN-Mn grid networks provides convincing evidence for the low-dimensional nature of these films.

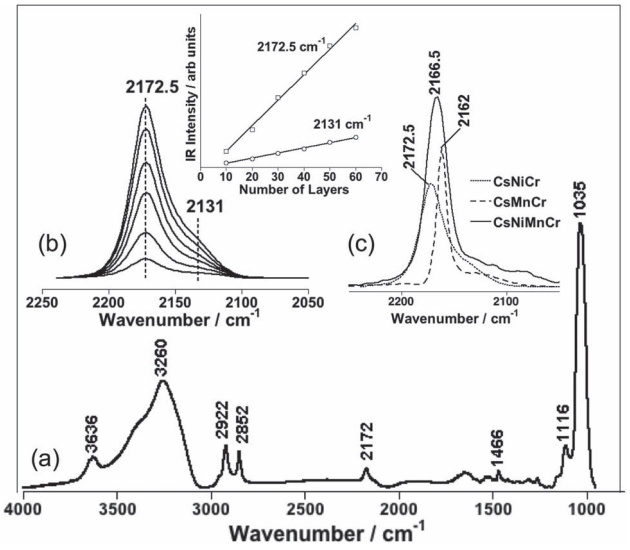

Figure 5. a) Infrared spectrum of a 20 layer thick hybrid DODA–clay–CsNiCr film transferred onto CaF_2 plates at a surface pressure of 10 mN m^{-1} and for a clay concentration in the subphase of 10 mg dm^{-3}; b) ν(CN) region for different number of DODA–clay–CsNiCr layers (from 10 to 60 layers) (the inset shows the relation between the IR intensity and the number of layers); c) ν(CN) region for the different 40-layer hybrid DODA–clay–PBA films.

However, not considering the absolute intensity, the magnetization data for both orientations were basically the same. Therefore, we present here the measurements obtained for the parallel direction. **Figure 6** shows the field-cooled (FC) and zero-field-cooled (ZFC) magnetization for 120-layer hybrid films of DODA–montmorillonite–PBA where the PBA is CsNiCr (Figure 6a), CsMnCr (Figure 6b) and CsNiMnCr (Figure 6c). At first glance, the FC magnetization data seem to reveal the occurrence of a magnetic order in the thin-film structure with Curie temperatures of 80 K (CsNiCr and CsNiMnCr) and 65 K (CsMnCr) as determined by extrapolation of the steepest slope of the magnetization curves to $M = 0$. However, the zero-field-cooled (ZFC) magnetization curves show irreversibility below $T_{irrev} \approx 60$ K for CsNiCr and 55 K for CsMnCr, suggesting lower T_C values than those observed from the field-cooled (FC) magnetization curves. The ZFC magnetization curve for CsMnNiCr suggests the presence of two different magnetic orders around 40 K and 68 K, consistent with the presence of two different layers in the film (CsNiCr and CsMnCr). These T_C values are lower than those observed for the pure 3D bulk sample of the same material (T_C = 90 K for CsNiCr and CsMnCr).[33] However, the hysteresis loops measured at 2 K (insets of Figures 5a–c) show coercive fields of around 105 G, 75 G, and 130 G for CsNiCr, CsMnCr, and CsNiMnCr hybrid films, i.e., similar to those observed for pure 3D bulk samples.

Figures 7a–c show the alternating-current (AC) susceptibility measurements. The data show both χ' (real or absorptive) and χ'' (imaginary or dispersive) components with maxima at much lower temperatures than T_C, which are frequency-dependent. The presence of a χ'' component is indicative of uncompensated moments and the frequency dependence of the position of the maxima in both components suggests a spin-glass-like behavior. Spin-glass behavior results from contributions of randomness (i.e., site disorder, bond disorder, etc.) and mixed interactions (i.e., ferro- and antiferromagnetic coupling) within a material.[34] The combination of randomness and competing ferro- and antiferro-magnetic couplings between nearest-neighbor spin sites leads to spin frustration. In this respect, Figure 2 (B and E) shows the possible randomness and different magnetic couplings in these

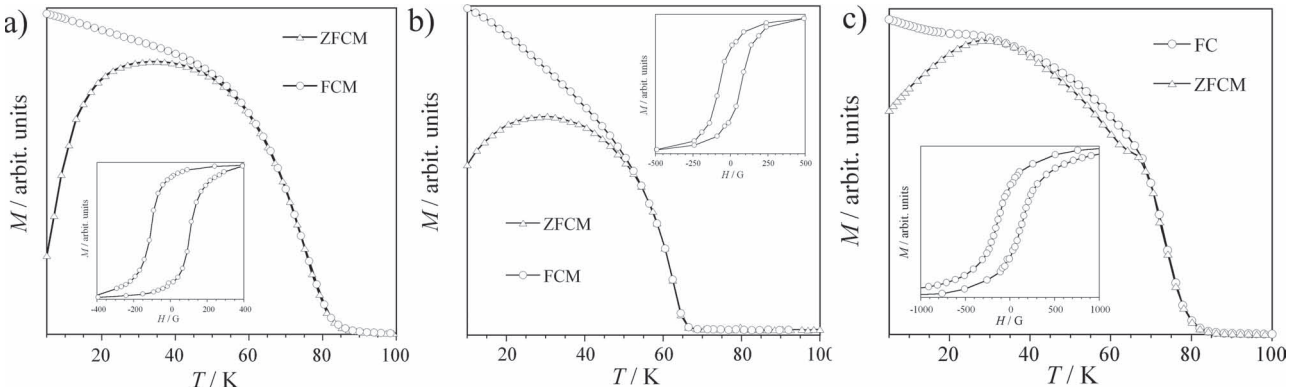

Figure 6. The field-cooled (FC) and zero-field-cooled (ZFC) magnetization for 120-layer hybrid films of DODA–clay–CsNiCr (a), DODA–clay–CsMnCr (b), and DODA–clay–CsNiMnCr (c) when the external field of 100 G is parallel to the film plane. Insets show hysteresis loops for the same films measured at 2 K.

films, which supports the idea of a spin-glass behavior. The freezing temperature, T_f, of the spin-glass is best determined by the maximum of χ' at the lowest frequency (1 Hz) closest to the zero-field limit. Following this method, the observed values of T_f are 48 K (CsNiCr) and 45 K (CsMnCr), which are much lower than the ordering temperature approximated from FC magnetization data (82 K and 65 K). It is important to note that it is also observed a shoulder in χ'' at about 68 K for CsNiCr (see below).

Both χ' and χ'' have two overlapping peaks for CsNiMnCr. There is no resolvable frequency dependence in the position of the higher temperature peak at 68 K, but there is frequency dependence in the lower temperature peak that is clearly resolved in χ''. This peak at lower temperature (Figure 7c) is very broad and must be a combination of two peaks, one of them corresponding to the CsNiCr layers and the other one to those of CsMnCr, which appear in this temperature region. The peak at higher temperature (68 K) must be related to the shoulder observed in χ'' for CsNiCr (Figure 7a) at the same temperature. The occurrence of a frequency-dependent transition below T_C is characteristic of the so-called "re-entrant spin-glass" behavior.[34] Some materials with spin-glass behavior exhibit their glass transition, T_f, at or above T_C. It is less common to see a glass transition below T_C and this behavior is termed "re-entrant" because the magnetically ordered state re-enters a "disordered" state at lower temperature. This is thermodynamically allowed only when the entropy of the frustrated spin system is reduced by creating cluster domains of spin with local order that are more weakly coupled to neighbouring cluster domains in a state of order similar to a true glass. In general, the frequency-dependence of the χ' and χ'' components in AC measurements indicate a slow magnetic relaxation of the magnetization.[34,35] Such behavior has been observed for single molecule magnets,[13,14,36–38] magnetic nanoparticles[39–41] as well as single-chain magnets,[15,16,42–45] but the same behavior also occurs in spin-glass systems.[34,35]

The associated relaxation time of the magnetization can be described by an Arrhenius law (equation (1)).[34,35]

$$\tau_r = \tau_0 \exp\left(\frac{E_0}{k_B T}\right) \quad (1)$$

During AC measurements of the magnetic susceptibility of the material, the maximum observed in the χ'' component (out-of-phase) corresponds to the blocking/glass temperature,

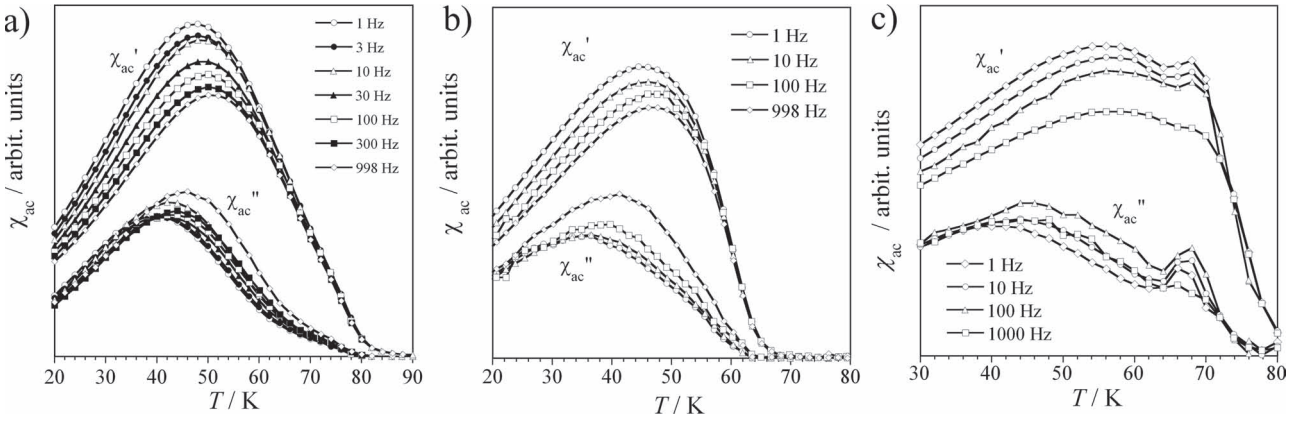

Figure 7. AC magnetic susceptibility for various frequencies in the 1–1000 Hz range for 120-layer hybrid films of: a) DODA–clay–CsNiCr, b) DODA–clay–CsMnCr, and c) DODA–clay–CsNiMnCr.

small NANO MICRO

T_B, at which the relaxation time is equal to the timescale of the measurement,[14,39–41,46] $\tau_0 = 1/2\pi f_0$, f_0 being the attempt or exciting frequency of the AC susceptometer, k_B the Boltzmann constant and T the absolute temperature.

If one plots ln τ versus $1/T$, the graphs can be well approximated by a purely linear fit (see Figure S1 of the SI for CsNiCr and CsMnCr), meaning that the behavior follows the Arrhenius law [Equation (1)]. However, the fits give unphysical values for τ_0 (~10^{-20} s for CsNiCr and ~10^{-22} s for CsMnCr), well above typical relaxation values of ~10^{-9}–10^{-12} s for superparamagnets. These very low and unphysical values of τ_0 suggest that not only one energy barrier exists but a large number of them and therefore disordered ferro- (CsNiCr) and ferri-magnets (CsMnCr) occur in the films. In fact, very low values for τ_0 are obtained ($\tau_0 \approx 10^{-30}$–10^{-40} s) when Equation (1) is applied to spin-glasses.[34,35] The existence of a large distribution of relaxation times can be also observed from the difference between T_{irrev} and T_C. The larger is the difference, the larger the distribution of relaxation times. In molecular nanomagnets these two temperatures have very close values. In this context, Mydosh[34] has proposed the F ratio to distinguish between a spin-glass and superparamagnetic state (Equation 2), where T_i and T_j are the temperatures at which the maxima in χ'' at the frequencies f_i and f_j occur.

$$F = (T_i - T_j)/[T_i(\log f_i - \log f_j)] \quad (2)$$

We calculated the F values from Equation (2) for our hybrid films based on the data displayed in Figure 7a and b and found $F \approx 0.05$ for the CsNiCr and CsMnCr films (plot Figure S1 of the SI). These values testify for a spin-glass behavior ($F \approx 0.08$–0.001), value of $F \approx 0.3$–0.15 would be observed for superparamagnets.[34,35,47,48]

As suggested by Kim et al.,[39] who got a similar result for magnetic nanoparticles, the reason of this physical mismatch could be due to an increased interaction between entities owed to a morphological parameter leading to an increased anisotropy energy barrier. We therefore speculate that a dense PBA layer between clay platelets, or a clay - PBA interaction could be responsible for this increased interaction between magnetic entities; the sample could then be almost 2D and "weakly" superparamagnetic or a mixed superparamagnetic spin-glass. The latter hypothesis is supported by reports of Talham et al.[47–49] on similar PBA thin-film systems.

The magnetic behavior of our hybrid DODA–clay–PBA films is therefore radically different from that of the bulk 3D ferromagnetic PBA. Through the "on surface" synthesis the dimensionality of the compound reduced from 3D to 2D-like behavior. Moreover, to the best of our knowledge, the obtained glass temperatures for our various structures are as much as 40 K higher than all previously published values for similar compounds.

4. Conclusion

The use of a modified Langmuir–Schaefer approach combined with "on surface" synthesis of organometallic molecule-based magnetic compounds enabled the synthesis of Prussian Blue Analogue structures with reduced dimensionality separated by layers of nanosized clay platelets. These low-dimensional PBA-based structures show new magnetic properties between superparamagnetic and spin-glass properties with high blocking glass temperatures above 65 K.

Supporting Information

Supporting Information is available from the Wiley Online Library or from the author.

Acknowledgements

We thank Dr. Serena Margadonna for insightful discussions in the early stage of this project. L.M.T. acknowledges E.U. support through the EIF-041956 Marie Curie fellowship. This work was performed within "Top Research School" program of the Zernike Institute for Advanced Materials under the Bonus Incentive Scheme (BIS) of the Netherlands'Ministery of Education, Science, and Culture and received financial support from the Dutch Foundation for Fundamental Research on Matter (FOM) as well as the Ministerio Español de Ciencia y Tecnologia through the project Consolider Ingenio CSD-2007-00010 (Molecular Nanoscience). Part of this work was supported by funding from the ERC grant (FP7) N°246791–COUNTATOMS.

[1] S. Ferlay, T. Mallah, R. Ouahes, P. Veillet, M. Verdaguer, *Nature* **1995**, *378*, 701–703.
[2] E. Dujardin, S. Ferlay, X. Phan, C. Desplanches, C. Cartier dit Moulin, P. Sainctavit, F. Baudelet, E. Dartyge, P. Veillet, M. Verdaguer, *J. Am. Chem. Soc.* **1998**, *120*, 11347–11352.
[3] Ø. Hatlevik, W. E. Buschmann, J. Zhang, J. L. Manson, J. S. Miller, *Adv. Mater.* **1999**, *11*, 914–918.
[4] S. M. Holmes, G. S. Girolami, *J. Am. Chem. Soc.* **1999**, *121*, 5593–5594.
[5] S. Margadonna, K. Prassides, A. N. Fitch, *J. Am. Chem. Soc.* **2004**, *126*, 15390–15391.
[6] T. T. A. Lummen, R. Y. N. Gengler, P. Rudolf, F. Lusitani, E. J. M. Vertelman, P. J. van Koningsbruggen, M. Knupfer, O. Molodtsova, J.-J. Pireaux, P. H. M. van Loosdrecht, *J. Phys. Chem. C* **2008**, *112*, 14158–14167.
[7] D. Li, R. Clérac, O. Roubeau, E. Harté, C. Mathonière, R. Le Bris, S. M. Holmes, *J. Am. Chem. Soc.* **2008**, *130*, 252–258.
[8] L. Egan, K. Kamenev, D. Papanikolaou, Y. Takabayashi, S. Margadonna, *J. Am. Chem. Soc.* **2006**, *128*, 6034–6035.
[9] O. Sato, T. Iyoda, A. Fujishima, K. Hashimoto, *Science* **1996**, *272*, 704–705.
[10] H. W. Liu, K. Matsuda, Z. Z. Gu, K. Takahashi, A. L. Cui, R. Nakajima, A. Fujishima, O. Sato, *Phys. Rev. Lett.* **2003**, *90*, 167403.
[11] D. M. Guldi, F. Zerbetto, V. Georgakilas, M. Prato, *Acc. Chem. Res.* **2005**, *38*, 38–43.
[12] N. A. Kotov, I. Dékány, J. H. Fendler, *Adv. Mater.* **1996**, *8*, 637–641.
[13] R. Sessoli, D. Gatteschi, A. Caneschi, M. A. Novak, *Nature* **1993**, *365*, 141–143.

[14] R. Sessoli, H. L. Tsai, A. R. Schake, S. Wang, J. B. Vincent, K. Folting, D. Gatteschi, G. Christou, D. N. Hendrickson, *J. Am. Chem. Soc.* **1993**, *115*, 1804–1816.
[15] R. Lescouezec, L. Toma, J. Vaissermann, M. Verdaguer, F. Delgado, C. Ruiz-Perez, F. Lloret, M. Julve, *Coord. Chem. Rev.* **2005**, *249*, 2691–2729.
[16] L. Toma, R. Lescouezec, J. Pasan, C. Ruiz-Perez, J. Vaissermann, J. Cano, R. Carrasco, W. Wernsdorfer, F. Lloret, M. Julve, *J. Am. Chem. Soc.* **2006**, *128*, 4842–4853.
[17] O. Sato, T. Iyoda, A. Fujishima, K. Hashimoto, *Science* **1996**, *272*, 704–705.
[18] Y. Umemura, *J. Phys. Chem. B* **2002**, *106*, 11168–11171.
[19] K. Tamura, H. Setsuda, M. Taniguchi, A. Yamagishi, *Langmuir* **1999**, *15*, 6915–6920.
[20] A. Yamagishi, Y. Umemura, K. Tamura, K. Inukai, *Kobunshi Ronbunshu* **2000**, *57*, 311–323.
[21] Y. Umemura, A. Yamagishi, R. Schoonheydt, A. Persoons, F. De Schryver, *J. Am. Chem. Soc.* **2002**, *124*, 992–997.
[22] J. Kawamata, S. Hirakawa, S. Tani, Y. Ogata, A. Yamagishi, *J. Nonlinear Opt. Phys. Mater.* **2004**, *13*, 355–358.
[23] Y. Umemura, A. Yamagishi, R. Schoonheydt, A. Persoons, F. De Schryver, *Langmuir* **2001**, *17*, 449–455.
[24] Y. Umemura, Y. Einaga, A. Yamagishi, *Mater. Lett.* **2004**, *58*, 2472–2475.
[25] L. M. Toma, R. Y. N. Gengler, D. Cangussu, E. Pardo, F. Lloret, P. Rudolf, *J. Phys. Chem. Lett.* **2011**, *2*, 2004–2008.
[26] L. Toma, R. Gengler, E. Prinsen, D. Gournis, P. Rudolf, *Phys. Chem. Chem. Phys.* **2010**, *12*, 12188–12197.
[27] Y. Umemura, *J. Phys. Chem. B* **2002**, *106*, 11168–11171.
[28] Y. Umemura, Y. Onodera, A. Yamagishi, *Thin SolidFlms* **2003**, *426*, 216–220.
[29] T. L. Barr, *Appl. Surf. Sci.* **1983**, *15*, 1–35.
[30] T. Yamamoto, Y. Umemura, O. Sato, Y. Einaga, *Chem. Mat.* **2004**, *16*, 1195–1201.
[31] T. Yamamoto, Y. Umemura, O. Sato, Y. Einaga, *Chem. Lett.* **2004**, *33*, 500–501.
[32] T. Yamamoto, Y. Umemura, O. Sato, Y. Einaga, *J. Am. Chem. Soc.* **2005**, *127*, 16065–16073.
[33] V. Gadet, T. Mallah, I. Castro, M. Verdaguer, P. Veillet, *J. Am. Chem. Soc.* **1992**, *114*, 9213–9214.
[34] J. A. Mydosh, *Spin Glasses: an Experimental Introduction*, Taylor & Francis, London, UK **1993**.
[35] K. Binder, A. P. Young, *Rev. Mod. Phys.* **1986**, *58*, 801–976.
[36] J. J. Sokol, A. G. Hee, J. R. Long, *J. Am. Chem. Soc.* **2002**, *124*, 7656–7657.
[37] J. Yoo, E. K. Brechin, A. Yamaguchi, M. Nakano, J. C. Huffman, A. L. Maniero, L.-C. Brunel, K. Awaga, H. Ishimoto, G. Christou, D. N. Hendrickson, *Inorg. Chem.* **2000**, *39*, 3615–3623.
[38] D. Gatteschi, R. Sessoli, J. Villain, *Molecular Nanomagnets*, Oxford University Press, Oxford, UK **2006**.
[39] D. K. Kim, Y. Zhang, W. Voit, K. V. Rao, M. Muhammed, *J. Magn. Magn. Mater.* **2001**, *225*, 30–36.
[40] K. Mohan Kant, K. Sethupathi, M. S. Ramachandra Rao, *J. Appl. Phys.***2008**, *103*, 07D501.
[41] F. Bødker, S. Mørup, M. S. Pedersen, P. Svedlindh, G. T. Jonsson, J. L. Garcia-Palacios, F. J. Lazaro, *J. Magn. Magn. Mater.* **1998**, *177–181*, 925–927.
[42] E. Pardo, R. Ruiz-Garcia, F. Lloret, J. Faus, M. Julve, Y. Journaux, F. Delgado, C. Ruiz-Perez, *Adv. Mater.* **2004**, *16*, 1597–1600.
[43] E. Pardo, R. Ruiz-García, F. Lloret, J. Faus, M. Julve, Y. Journaux, M. A. Novak, F. S. Delgado, C. Ruiz-Pérez, *Chem. Eur. J.* **2007**, *13*, 2054–2066.
[44] E. Pardo, C. Train, R. Lescouëzec, Y. Journaux, J. Pasán, C. Ruiz-Pérez, F. S. Delgado, R. Ruiz-Garcia, F. Lloret, C. Paulsen, *Chem. Commun.* **2010**, *46*, 2322–2324.
[45] J. Ferrando-Soria, D. Cangussu, M. Eslava, Y. Journaux, R. Lescouëzec, M. Julve, F. Lloret, J. Pasán, C. Ruiz-Pérez, E. Lhotel, C. Paulsen, E. Pardo, *Chem. Eur. J.* **2011**, *17*, 12482–12494.
[46] D. E. Freedman, W. H. Harman, T. D. Harris, G. J. Long, C. J. Chang, J. R. Long, *J. Am. Chem. Soc.* **2010**, *132*, 1224–1225.
[47] J. Culp, J. Park, M. Meisel, D. Talham, *Inorg. Chem.* **2003**, *42*, 2842–2848.
[48] J. Culp, J. Park, D. Stratakis, M. Meisel, D. Talham, *J. Am. Chem. Soc.* **2002**, *124*, 10083–10090.
[49] J. Culp, J. Park, I. Benitez, M. Meisel, D. Talham, *Polyhedron* **2003**, *22*, 2125–2131.

Received: March 8, 2012
Published online: July 3, 2012

